Dissertation for Master of Science

Event Related Analysis and Code Implementation of Functional Near Infrared Spectroscopy (fNIRS)

Yi Wang
2502033

Supervised by Felipe Orihuela-Espina

School of Computer Science
University of Birmingham

September 2023

Abstract

When scientists attempt to isolate the effects of a single stimulus from the signals of brain regions that receive multiple evoked stimuli, the existing methods are high complex. To help neuroscientists use this approach more easily, this dissertation implements an existing event-related model into a new optical neuroimaging data analysis tool. A general linear model is used for comparison, and regression analyses are performed on synthetic signals and functional near-infrared spectroscopy instrumental acquisition data. The accuracy of the ER model is confirmed. It was found that the ER model had superior decoupling capability in the implemented code, but not all subjects preferred the ER model.

Acknowledgements

From the bottom of my heart, I would like to extend my sincerest gratitude to my supervisor, Dr. Orihuela-Espina. I appreciate his selfless patience and enthusiasm in helping me to overcome lots of challenging problems.

I want to express my gratitude to my parents, Zhenhua Sun and Yunshen Wang. Their love has been my strongest driving force throughout this journey.

Lastly, I'd like to thank my two dear dogs, Zaizai and Daxiong.

Contents

List of Figures

List of Tables

Chapter 1

Introduction

This chapter outlines the motivation and aim of this dissertation and ends with a brief overview of each chapter.

1.1 Motivation

Functional near-infrared spectroscopy (fNIRS) has become more widely accepted and used in cognitive neurology over recent decades. This is due to the higher portability, comfort and better temporal resolution of fNIRS in comparision to other neuroimaging techniques such as fMRI (Pinti et al., 2019). fNIRS is applicable to a wide range of subjects populations, evidenced by numerous studies ranging from infants to adults to the elderly (Zhang et al., 2019; Li et al., 2021; Maidan et al., 2015). These numerous studies are not lacking in experiments specifically designed to study the effects of different stimuli on the cerebral vasculature (Uga et al., 2014; Plichta et al., 2007). In these studies, the experiments are structured to quickly transition between multiple stimuli in order to study human perceptions of a single stimulus, which is referred to as event-related analysis.

Event-related analyses are widely used to do regression analyses based on general linear models to separate the brain activity triggered by a single stimulus from multiple stimuli. While this method offers greater precision, it is also more intricate (Pinti et al., 2019). This is due to the addition of first order derivatives and second order derivatives to the classical GLM model (Çiftçi et al., 2008). This is a popular and valuable method for dealing with event-related analyses; however, the code and experimental data associated with this method are not yet available in the published literatures. There are already a number of toolkits dedicated to fNIRS

that are equipped to handle event-related analyses, such as NIRS-SPM (Ye et al., 2009). However, the options remain limited, somewhat constraining researchers in their selection of analysis tools.

1.2 Aim and Research Questions

The aim of this study was to implement an existing event-related model, transforming it into a tool for ER analyses on the fNIRS dataset, and apply it to a surgeon's dataset. Due to time constraints, the study concentrated on performing the analyses sole at the single subject level. Before directly utilizing the experimental data, however, it was necessary to asses the accuracy of the implemented ER model by using the traditional GLM model for comparison. The surgeon's dataset comprised data from multiple subjects. Therefore, the first and the second research question was focused on, respectively:

1. When multiple stimuli overlap in rapid succession, and regression analyses are conducted using both the GLM model and the ER model as implemented in the code, which model more accurately differentiate the effects of individual stimuli on brain regions?

   To address this question, synthetic data will be used in the study. Regression analyses will be conducted on both models using the same brain activity signals and stimulus sequences in the context of known designs and channel response situations. It is hypothesized that the ER model can better decouple the neural responses of the brain to the evoked task.

2. Within the actual collected fNIRS data set, when decoupling the active brain signals under multiple stimuli using both the ER model and the GLM model, is there consistency between the two models across different subjects?

   To respond to this question, a significance test will be conducted for each channel of every subject in the collected data, and the results will be graphically presented. Two representative subjects will be selected to assess the consistency between the models. In the hypothesis, the channel activity between the two models will remain consistent across subjects.

1.3 Dissertation structure

This dissertation contains five chapters. The first chapter introduces the motivation, objectives, and hypotheses of the reported study are introduced. The second chapter provides a literature review. Firstly, for the sake of later reading, the meaning of hemodynamic response function and general linear model are briefly introduced. fthe present general fNIRS data preprocessing procedure and statistical analysis methods are described, respectively. Finally the research contributions are stated. The data sources are briefly summarised in the methodology in chapter three. The steps for generating synthetic data, pre-processing and analysing the collected data are highlighted. Chapter 4 gives a graphical presentation of the previous steps, divided into synthesising data and collecting data. Further more, chapter five gives a discussion of the results of the previous chapter. Lastly, in chapter six, the research questions from chapter one are answered and the whole text is summarised.

Chapter 2

Literature Review

This chapter contains a literature review of previous work. Firstly, basic information about fNIRS, acquisition methods and signal processing techniques are presented. Then the data analysis methods commonly used in the early and current phases of fNIRS are described. An overview of block and event-related designs commonly used for experiments is given. Finally, a brief statement of the research gap is given.

2.1 Functional Near-Infrared Spectroscopy

Functional near-infrared spectroscopy is a non-invasive neuroimaging technique that measures changes in the concentration of oxygenated and deoxygenated hemoglobin after neurons have been stimulated (Quaresima et al., 2012; Pinti et al., 2020). The instrument is shown as Figure 2.1.

This is because of the hemodynamic response that occurs within the brain region when stimuli are received (Quaresima et al., 2012). That is, in order to generate brain activity, neurons have an increased need for nutrients in blood transport, such as oxygen. Thus large amounts of oxygen are transported to the activated brain area, and oxygen is transported by haemoglobin. As a result, the oxygenated haemoglobin in the local brain region greatly exceeds the deoxygenated haemoglobin when stimulation is received (Pinti et al., 2020).

Figure 2.1: A woman is wearing an fNIRS system on her head to measure the signals in the covered brain area (Cortechsolutions, 2022).

2.1.1 Acquisition of brain region data

A FNIRS device consists of a set of light sources and detector that are placed on the participant's scalp (Scarpa et al., 2013). As shown in Figure 2.2, Near-infrared light travels from a light source and gets scattered as it passes through biological tissues. Some of this light that passes through the multiple tissue layers of the head, such as the scalp, skull and cerebrospinal fluid, and is finally picked up by the detector forms a semi-circular path that looks like a banana shape (Pinti et al., 2020; Yoo et al., 2023). The usual distance between optode is 2.5cm-3.5cm (Quaresima et al., 2012; Scarpa et al., 2013), and the optode distance is different for infants and adults, with a case study using a distance of 2cm when measuring signals of activity in infants' brain regions (Weibley et al., 2021). On the other hand, the choice of the distance between the optode also has to consider the variation of the signal to noise ratio. The greater the distance between the light source and the detector, the longer and deeper the path travelled by the light, but more photons are absorbed and hence limits the amount of signals (Quaresima et al., 2012).

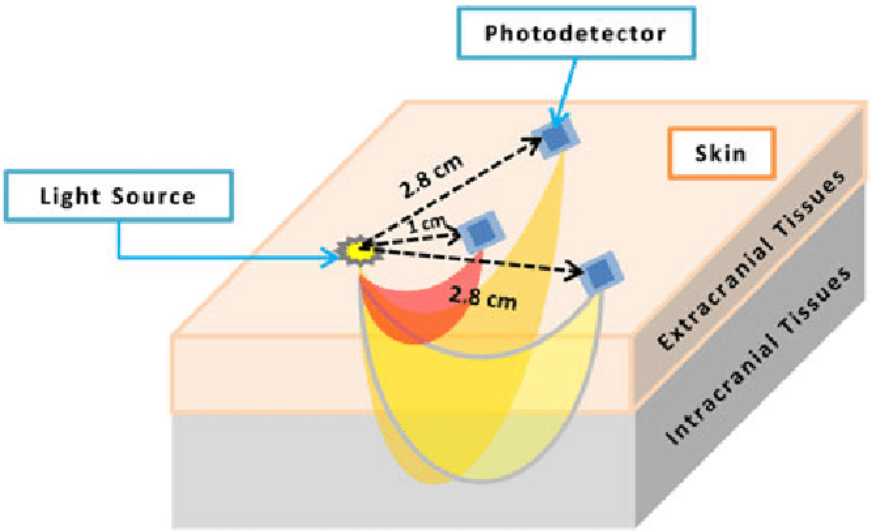

Figure 2.2: Schematic diagram of the light path: from the light source through the scalp back to the detector (Barati et al., 2012).

During the movement of photons, they are scattered, reflected and absorbed (Almajidy et al., 2020). Human tissues absorb NIR light at different wavelengths differently. As shown in Figure 2.3, water absorbs NIR light greatly at wavelengths above 900 nm. When the wavelength is 700nm 900nm, oxyhemoglobin and deoxyhemoglobin have greater absorption of near-infrared light, and water has a lower absorption capacity for near-infrared light. Therefore, the study considers the range from 700nm to 900nm as a "optical window" (Len-Carrin & Len-Domnguez, 2012). Within the spectral window, the different absorptions of the two hemoglobins give scientists the possibility to calculate the changes in their concentrations.

2.1.2 The modified Beer-Lambert Law

Light attenuates as it is emitted and received. After obtaining brain activity signals, the modified Beer-Lambert Law allows the calculation of the changes in the concentration of both oxyhemoglobin and deoxyhemoglobin before and after light attenuation (Quaresima et al., 2012; Len-Carrin & Len-Domnguez, 2012; Almajidy

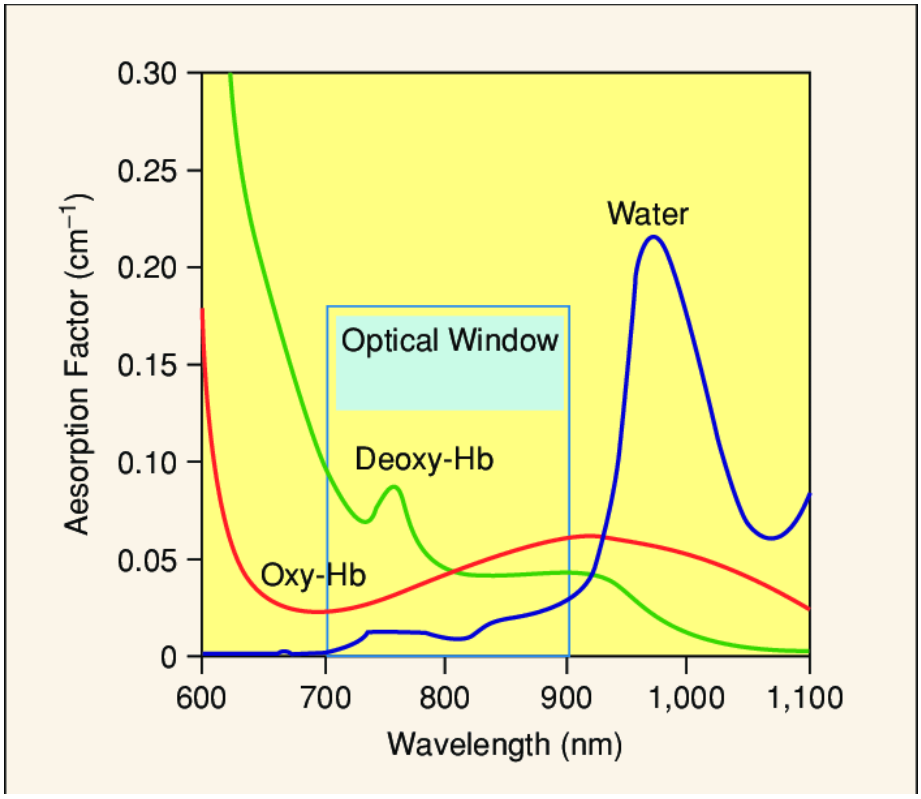

Figure 2.3: In the range of the optical window, the absorption of near-infrared light by water is very low, while the more light absorbing substance is hemoglobin (Izzetoglu et al., 2007).

et al., 2020):

$$A = a \cdot c \cdot d \cdot DPF + G. \tag{2.1}$$

Equation 1.1 shows the relationship between several parameters related to loss of light intensity, where ε denotes the molar extinction coefficient at wavelength λ; c denotes the concentration of chromophores; d denotes the distance from the source to the detector; DPF denotes the Differential Path Length Factor, which explains the length of light propagation before it returns to the receiver; G denotes the loss of photons due to dispersion; and A denotes the attenuation of the light intensity.

We can obtain the dependent variable ΔA varying with Δt by $\Delta A(\lambda) = A(\lambda)$ with $t_1 - A(\lambda)$ with t_0:

$$\Delta A(\lambda) = \varepsilon(\lambda) \cdot \Delta c \cdot d \cdot DPF(\lambda). \tag{2.2}$$

Equation 2.2 we have obtained the relationship between ΔA and Δc. Therefore the equations for the change in the concentrations of oxyhemoglobin and deoxyhemoglobin with time t are respectively:

$$\Delta HbO = \frac{\varepsilon_{HbR}(\lambda_2) \cdot \frac{\Delta OD(\lambda_1)}{d \cdot DPF(\lambda_1)} - \varepsilon_{HbR}(\lambda_1) \cdot \frac{\Delta OD(\lambda_2)}{d \cdot DPF(\lambda_2)}}{\varepsilon_{HbO}(\lambda_1) \cdot \varepsilon_{HbR}(\lambda_2 - \varepsilon_{HbO}(\lambda_2) \cdot \varepsilon_{HbR}(\lambda_1)}, \tag{2.3}$$

$$\Delta HbR = \frac{\varepsilon_{HbO}(\lambda_1) \cdot \frac{\Delta OD(\lambda_2)}{d \cdot DPF(\lambda_2)} - \varepsilon_{HbO}(\lambda_2) \cdot \frac{\Delta OD(\lambda_1)}{d \cdot DPF(\lambda_1)}}{\varepsilon_{HbO}(\lambda_1) \cdot \varepsilon_{HbR}(\lambda_2) - \varepsilon_{HbO}(\lambda_2) \cdot \varepsilon_{HbR}(\lambda_1)}. \tag{2.4}$$

2.2 Hemodynamic Response Function

In order to generate brain activity, neurons need nutrients to produce energy. Oxygen is transported by hemoglobin. During the process that occurs in the brain in response to a stimulus, there is a rise in the concentration of oxygenated haemoglobin in the blood, and a fall in the concentration of deoxygenated hemoglobin in the active regions of the brain. This process is known as the hemodynamic response (Pinti et al., 2018). The hemodynamic response function generally consists of two components, the first term is the positive signal change from the start of the stimulus to the peak of the function, and the second term is the negative signal change from the end of the stimulus to the peak of the function's undershoot. The first peak delay is about 4s to 6s and the second peak delay is about 6s to 10s (Mayer et al., 2014).

2.3 Processing

The studies by Pinti et al. (2019) and Hocke et al. (2018) have clearly suggested that there is a lack of standards and uniformity in the processing steps for fNIRS neuroimaging data nowadays. This means that different researchs may get various results when processing the same group of data. There has been some literature summarising the common processing steps used for fNIRS in recent years. For example, Dans et al. (2021) statistically identified that the most commonly used processing techniques in the decade from 2010 to 2020 are filters.

Signal quality is affected by a variety of factors such as instrumental noise, physiological noise, environmental noise, and motion artefacts. They usually present as sharp peak variations, which leads to errors in the following analyses of the data

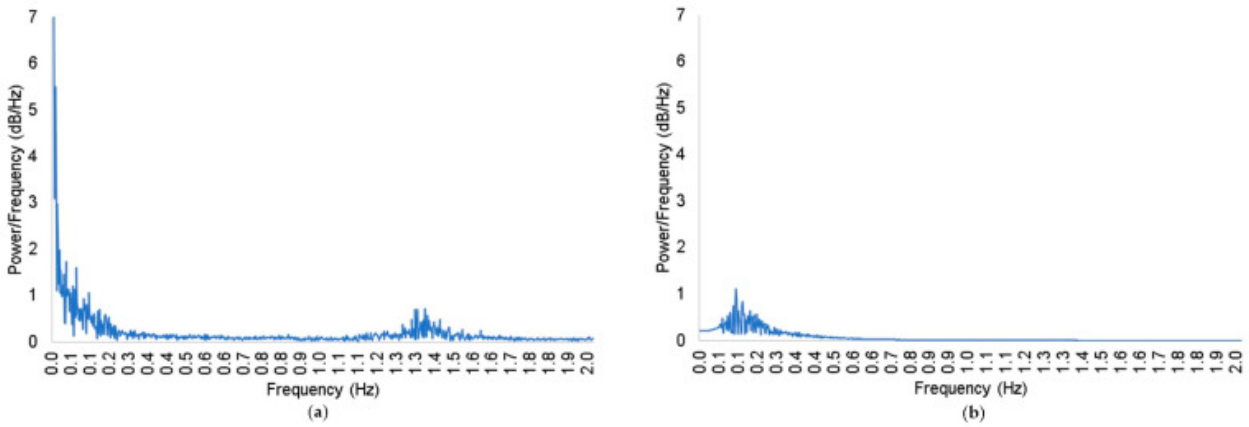

Figure 2.4: Figure (a) represents the display of the Fourier's spectral decomposition of unfiltered data. Figure (b) shows the data after using a bandpass filter with a range of 0.01 to 0.4 (Dans et al., 2021).

(Hocke et al., 2018). When performing processing, it is most common to first visually check the strength of the raw data (Pinti et al., 2019). The signals in the channel were observed during visual inspection to see if there was a distinct and sustained heartbeat, which implies that the variation of light intensity in the channel is strongly influenced by hemodynamic change and has a high signal-to-noise ratio. However, this is a very subjective technique and it takes a long time and is slow to operate. Setting parameters such as signal-to-noise ratio threshold, coefficient of variation, etc. for the channel is a more systematic method (Hocke et al., 2018). As mentioned earlier, some physiological noises can also pollute the signal, such as respiratory and cardiac impulse, it is quite common and straightforward to use filtering to remove the noise. Bandpass filter set the frequency range of the cut-off signal, allowing signals of a specific frequency to pass through while attenuating signals outside the range, thereby attenuating intrusive instrumental and physiological noise (Dans et al., 2021). An example has shown on Figure 2.4.

There is no criterion for the frequency range, in the paper published in 2016, a common range is [0.01, 0.5] Hz (Pinti et al., 2019). In addition, when a participant wears an fNIRS device for exercise, such as walking, the contact between the optodes and the head may be decoupled because it is not tight enough, which results in an interference of the light as it propagates through the tissues of the head. This is known as motion artefacts (Hocke et al., 2018). Motion artefacts behave differently. They can be high-frequency and sharp, or low-frequency and difficult to capture. When motion

artefacts are easily detected, the performance of spline interpolation is a common approach to deal with the. However, when motion artefacts are low-frequency and can be easily confused with HRFs, wavelet filters are popular (Brigadoi et al., 2014). Once the filtering is complete, the processed optical intensity data can be converted to optical density and then to oxyhemoglobin concentration and deoxyhemoglobin concentration for further analysis.

2.4 fNIRS data analysis methods

There was no relatively uniform signal processing procedure or suitable activation data extraction method in fNIRS studies. In the early, the relatively common method was to average the baseline period and the stimulus period of occurrence separately. A t-test was then used as an assessment method to verify whether the data were significantly different during the task (Tak & Ye, 2014). However, this approach does not account for the timing of the fNIRS data. Instead, the more general approach that considers the time process of the data is the general linear model. This method has been extensively researched in the fMRI field. In the GLM method, the brain activity signal is split into a linear combination of regressors (design matrix) and error terms. A hemodynamic response function is used to describe the actual hemodynamic response caused by brain neural activity (Uga et al., 2014).

The general linear model in fNIRS is a linear combination of multiple explanatory variables (von Lühmann et al., 2020). The expression is

$$\mathbf{Y} = \mathbf{X}\boldsymbol{\beta} + \varepsilon, \tag{2.5}$$

where the observed data $\mathbf{Y}$ is a TxC order matrix, implying that there are a total of C channels of collected data for each subject, each containing T fNIRS time data. $\mathbf{X}$ denotes the design matrix, which is a TxM order matrix, where M denotes the number of regressors. $\boldsymbol{\beta}$ is a parameter matrix representing the weight of the regressors on the contribution to the signal $\mathbf{Y}$. This can be estimated by the Ordinary Least Squares method:

$$\boldsymbol{\beta} = \left(\mathbf{X}^T\mathbf{X}\right)^{-1}\mathbf{X}^T\mathbf{Y}. \tag{2.6}$$

ε is an independent and normally distributed error term that represents the portion that cannot be explained by the GLM model (Plichta et al., 2007).

The design matrix plays an important role in the GLM model. Schroeter (2004)

implemented two experiments in his study. One was a checkerboard grid paradigm with 17 seconds of rest for every 18 seconds of stimulation performed, and one was a rotated letter as a paradigm for visual stimulation with 42 seconds of rest for every 18 seconds of stimulation. In the general linear model $Y=X*\beta+\varepsilon$, the design matrix consists of a sequence of stimuli, i.e., a boxcar function. In a one-sample analysis, a single subject did a t-test against a blank screen for each of the two stimuli to see if the level of activation was significant from zero. In group analyses, paired t-tests were performed on the activation of the two stimuli for all subjects. Finally, it was successfully demonstrated that the general linear model can be used for statistical analysis of optical imaging data. In contrast, Friston (1998), in his early work on event-related analysis of fMRI, introduced the derivative term of the hemodynamic response function into the design matrix of a general linear model to explain the displacement of the response in time. This technique has also been used in the field of fNIRS, where a blocked design was chosen for the research experiments of Uga et al. (2014). The design contained two continuous and consecutively alternating tasks. Oxygenated and deoxygenated hemoglobin were used as response variables in the study and changes in brain activity under both stimuli were analysed using GLM. The design matrix contains the HRF, the first-order derivative of the HRF, the second-order derivative of the HRF, and an intercept term, respectively. This allows the curve of the HRF to be adjusted in time to be more adapted to the hemodynamic response of different individuals. The figure has shown in Figure 2.5.

In addition to the block design described above, optical imaging studies also incorporate another common design method called an event-related design. Event-related designs allow the measurement of how the brain is affected by short duration stimuli and overlapping stimuli. In the study by Heilbronner and Münte (2013), each stimulus appeared for only 100 ms. Earlier, Plichta et al. (2007) showed that event-related model is more flexible than block analysis. This is because it usually takes more than 12 seconds for the hemodynamic response to return to the baseline state after a stimulus occurs, and any other stimulus that reappears before this time will lead to the appearance of a new hemodynamic response that overlaps with the previous one. To deal with the ER design of multiple stimulus cross-appearances occurring within a single HRF period, overlapping HRFs were handled using a general linear model. As previously mentioned, the inclusion of the first and second order derivatives of the HRF within the design matrix can regulate the start and end of the model to better capture the relationship between the stimulus and the signal. Thus, this design can contribute to some extent to decouple the changes in blood oxygen levels between

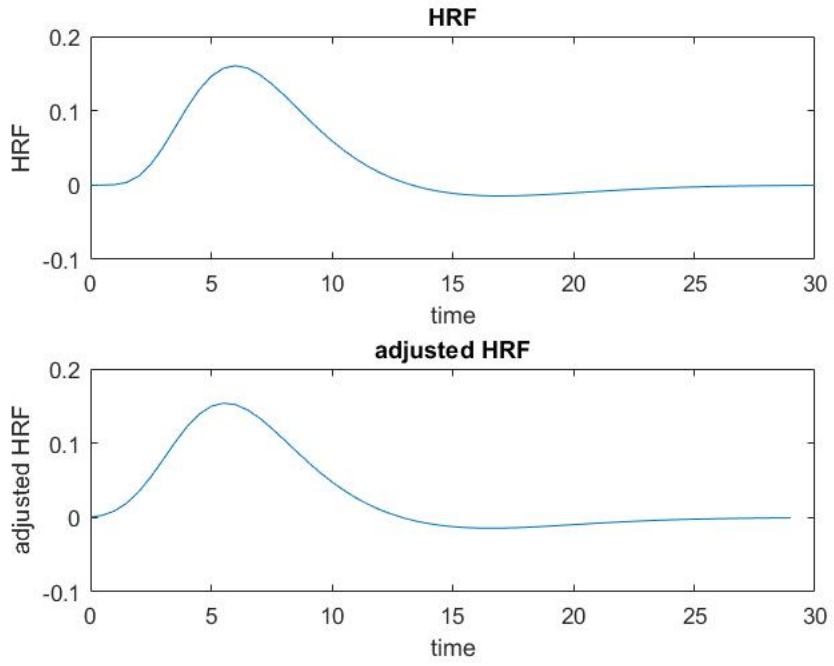

Figure 2.5: Canonical HRF and HRF with the addition of the derivative term.

different events. This study successfully demonstrated the strong applicability of the GLM-based modification model in analysing ER-designed fNIRS data. The same conclusion was reconfirmed in Ozawa et al. (2013), where the results of an ER design with a modified model based on GLM were similar to the fMRI results for the same experiment.

2.5 Research gap

While earlier researchers have made significant strides in event-related fNIRS models, the intricacy of their methods and the challenges in executing them have deterred neuroscientists from adopting this technology. Currently, there are toolboxes available, like NIRS-SPM (Ye et al., 2009), tailored for fNIRS that encompass this feature. However, the options are limited, and in order to provide researchers with a wider choice of analytical tools, the project attempts to implement models for event-related analysis into the new optical neuroimaging data processing toolbox, which allows sci-

entists to use different analytical tools for data processing and comparison of results.

Chapter 3

Methodology

This chapter states the steps taken to integrate the pre-existing event-related analysis model into the code. It starts with a brief overview of the data sources and optical probe placement. Next, the process of generating synthetic data for model validation is detailed. The subsequent section presents the pre-processing method for actual data. Finally, the methodology for conducting regression analyses on both the generated and pre-processed data using the general linear model and event-related model is clarified.

3.1 Experiments and data collection

The data for this project was provided by Dr Ronak Patel at Imperial College. A total of 28 participants took part in the experiment. Each participant completed three sessions of near-infrared spectroscopic measurements, with the first two sessions being completed within seven days, and participants returning a few weeks later for a final session of measurements. Two stimulus lines were included during each measurement, and each stimulus line performed four repetitive stimulation tasks of 10 s duration. Each participant had fNIRS data files for three measurements, and the three sessions were 'Pre', 'Post', and 'Retention'. There were two types of stimulation interventions: trans-cranial direct current stimulation (tDCS) and sham. Each intervention group included 14 participants. To be noted, Participant 2 had an interruption while taking the first 'Pre' session measurements, and here the data from the second measurements are used. Participant 25 did not take part in the third session of measurements, resulting in only two records for them.

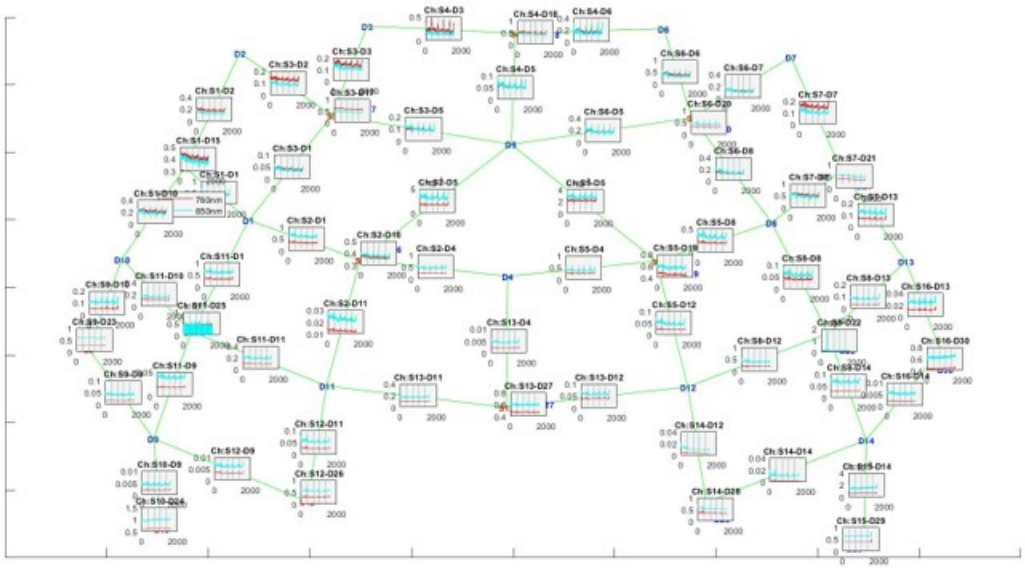

Figure 3.1: Display of optical poles and full-channel positions. The red line represents the 760 nm wavelength and the blue line represents the 850 nm wavelength.

3.2 Arrangement of optodes

Figure 3.1 illustrates the positioning of the optical pole on the scalp. With 16 sources and 30 detectors, the system allows for the measurement of 62 channels. Where the blue letter 'D' denotes the detector and the red letter 'S' denotes the source. Near infrared light is emitted at two wavelengths, 760 nm and 850 nm.

3.3 Synthetic data for model validation

Although it was mentioned in the literature review that there has been a significant amount of literature about event related analysis, there is still no literature that discloses code and experimental data, which makes it impossible to validate the model using the literature data. Therefore, before processing the real data, it's essential to generate synthetic data for the purposes of validating the new model on known ground truth. The objective was to compare the different ability of the code-implemented ER model to the classic GLM model with only one regressor for

the HRF to dissociate the effects of a single stimulus on the brain. Also, to verify whether the ER model implemented in the code can successfully decouple the effect of a single evoked stimulus on brain activity signals when two repetitive stimuli rapidly cross appear or overlap. Although this experimental design was block design but the length of the stimulation periods was so long that the regular GLM has been shown to fail due to saturation effects (Cignetti, 2016). In this sense, we hypothesized that the event related model may be able to adapt to this effect by modelling the saturated signal as the consequence of consecutive shorter stimulations train.

3.3.1 Generate the synthetic stimuli lines

As depicted in Figure 3.2, two independent stimulus lines were preset along with four channels corresponding to different brain regions. Each of these regions exhibited varied responses to the individual stimuli. Each stimulus line contained five blocks (tasks) with sufficient rest time between each task block. In the first block, stimulus 1 and stimulus 2 occurred and ended simultaneously. The start and end times of stimulus 2 of the fourth block were completely contained within the time period of stimulus 1. The two stimuli of the fifth block did not overlap at all. For the simulated channels, the first channel would have an active response to both stimuli, the second channel would respond only to stimulus 1, the third channel would respond only to stimulus 2, and the fourth channel would not respond to either stimulus.

3.3.2 Selection of a Hemodynamic Response Function (HRF)

In the study of Uga et al. (2014), it was mentioned that the use of a gamma function with two parameters as a hemodynamic response function can appropriately represent the hemodynamic response. The first and second parameters were set to 6s and 10s, representing the delay between the first peak and the second peak, respectively. The amplitude ratio of the first and second peaks was set to 6. The demonstration of HRF has displayed on Figure 2.5.

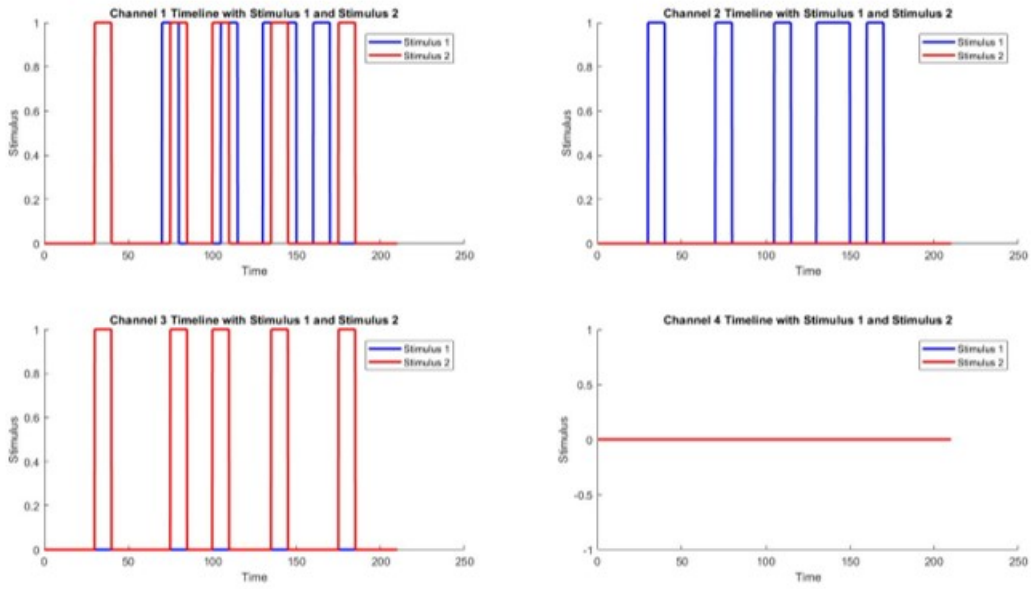

Figure 3.2: Demonstrate the response of the four channels to the stimuli. Boxcar pointing to 1 indicates that the brain receives the corresponding stimulus, and boxcar pointing to 2 indicates that the brain does not receive the stimulus.

3.3.3 Generating explanatory variables and response variables

Each stimulus line was treated as a boxcar and convolved with the hemodynamic response function to obtain the canonical HRF. The canonical HRF represents the trend of change in hemoglobin concentration. For the classical GLM model, the design matrix for each channel contains three columns: the convolution of stimulus 1 with HRF, the convolution of stimulus 2 with HRF, and the intercept term. As for the ER model design, the design matrix for each channel contains seven columns: convolution of stimulus 1 with HRF, convolution of stimulus 1 with the first order derivatives of HRF, convolution of stimulus 1 with the second order derivatives of HRF, convolution of stimulus 2 with HRF, convolution of stimulus 2 with the first order derivatives of HRF, convolution of stimulus 2 with the second order derivatives of HRF, and the intercept term. This step constructs the design matrix of the classcis GLM model and the ER model as explanatory variables.

The cumulative effect of multiple stimuli on cerebral nerves is reflected in the brain regional hemoglobin concentration. Hence, stimulus 1 and stimulus 2 were combined and convolved with the HRF to simulate brain activity signals under multiple stimuli, as illustrated in Figure 3.3.

Mayer Wave and Gaussian distribution noise were incorporated to more closely resemble actual data. The standard deviation of the Gaussian noise was set to 0.5^2 to control the noise intensity and fluctuation range. This step constructs the mock signal on Figure 3.4 and that will be used as the response variable.

3.4 Data processing pipeline

The flowchart illustrating data processing is presented in Figure 3.5. The majority of the processing steps can be accomplished in Matlab using functions from the Homer3 toolbox. Firstly draw a graph of the light intensity of all the channels and observe if there are any huge spikes, this determines whether or not to call the function in order to use the median filter to reduce the effect of noise. The next step is to prune the bad channels using the hmrR_PruneChannels function, set the range for the function's parameters using the percentile method. For example, choosing an upper bound of 95 and a lower bound of 5 and establishing that the data between 5% and 95% for a single parameter is valid, the function will exclude those channels

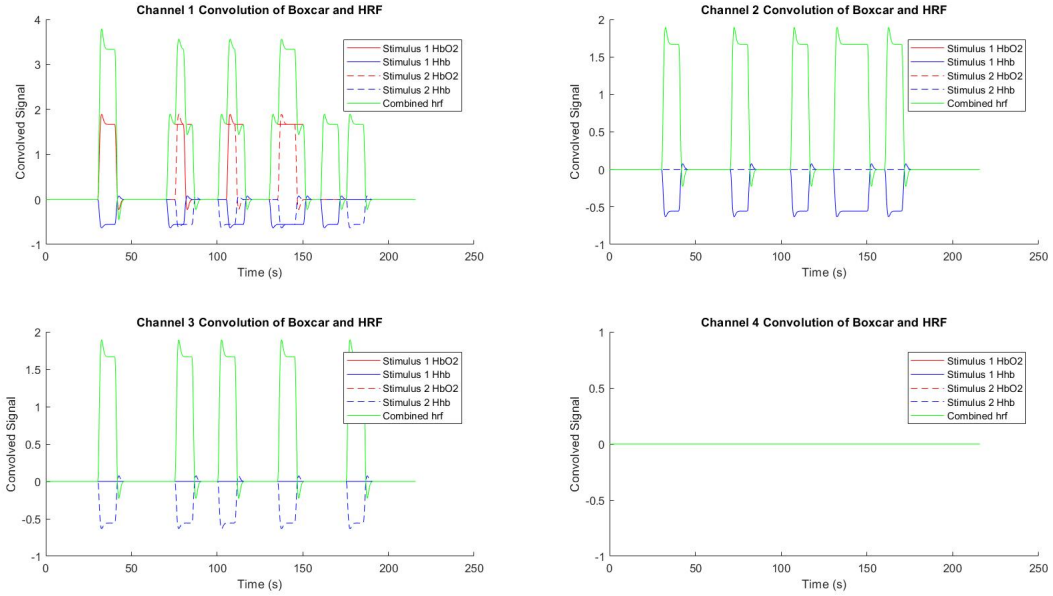

Figure 3.3: A diagram of hemoglobin concentration in the brain is generated. The green line represents the change in HbO concentration in brain regions after stimulation. The solid red line represents the HbO concentration during stimulus 1 alone; the dashed red line represents the HbO concentration during stimulus 2 alone; the solid blue line represents the HHb concentration during stimulus 1 alone; and the dashed blue line represents the HHb concentration during stimulus 2 alone.

outside the range. After pruning, draw again to check and modify the parameters or manually remove the missing bad channels. Next convert the light intensity to light density. The bandpass filter is then used to attenuate the signal beyond 0.01 Hz to 0.3 Hz, respectively. This signal cut-off range removes some physiological noise such as cardiac cycles.

In the next step, whether the function is called to detrend the filtered data depends on whether the signal has a overall significant upward or downward trend. The data from each channel was fit using a linear fit, and then the line of best fit was subtracted from the original data. The purpose of this step is to attenuate signal trends that are not related to a specific stimulus. Next motion artefacts are detected and corrected. This process is performed in one or more iterations depending on the

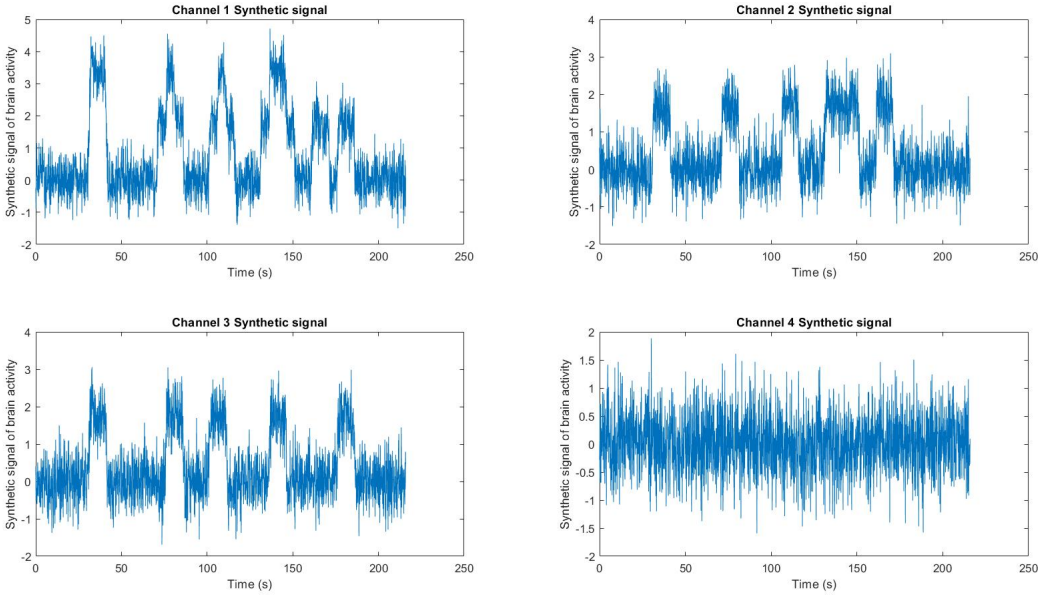

Figure 3.4: Synthetic signal with noise added.

intensity of the artefacts. It is important to note that motion artefacts are not completely eliminated and can only be minimised in order to secure most of the valuable information. As Figure 3.6 shown, the figure (a) is an example of a single channel with a few of motion artefacts marked in the red boxes and figure (b) shows the corrected optical density.

Finally, the refined optical density was converted to hemoglobin concentration as Figure 3.7 displayed.

3.5 Statistical methods and analyses

In section 3.3, synthetic data to be used for comparing the GLM model with the ER model has been created. To verify whether a stimulus is significant, a significance test needs to be done for each stimulus line per channel. The curve of the signal is made up of a large number of time points, so the slope of the points is found at each

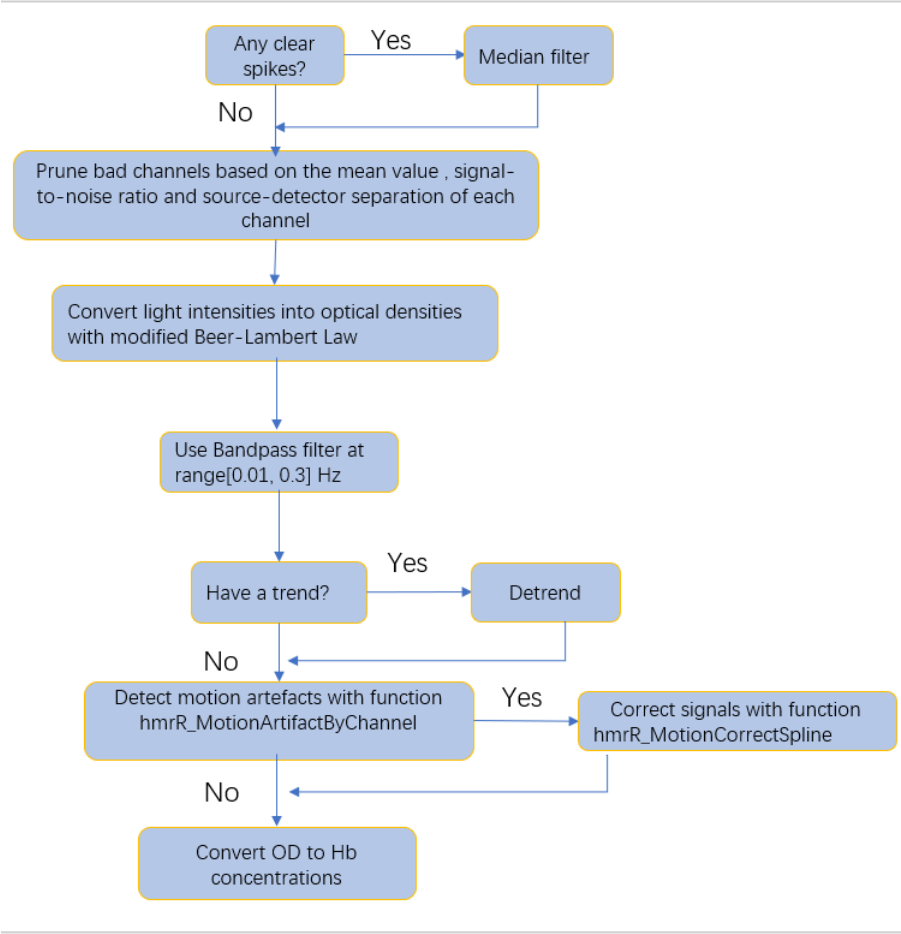

Figure 3.5: The processing flow chart.

time point. In the study of Plichta et al. (2007), the Ordinary Least Squares method was used to estimate the stimulus influence of the response signal. In matlab, the signal Y can be directly used to divide by the design matrix X. This is because for each time point, Equation 2.5 can be interpreted as: Y is the brain activity signal at a point, X is a row of the design matrix, β is the effect of the stimulus to be estimated, and ε is the residual. The purpose of the Ordinary Least Squares method is to minimise the sum of squares of the residuals. Therefore, to calculate β in Matlab, simply divide the response signal Y by the design matrix X. There are as many time points as there are slopes to get.

For both response variable and explanatory variable, the autocorrelation of the time

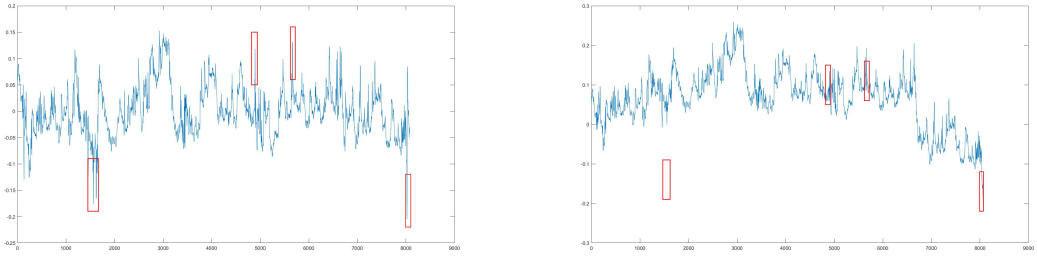

(a) Before correct the motion artefacts

(b) After correct the motion artefacts

Figure 3.6: The channel 5 data of subject 19 during the 'Pre' session serves as an example of corrected motion artefacts. Figure (a) is labelled with a few of red boxes where motion artefacts were detected. Corrected motion artefacts are labelled at the same location in Figure (b).

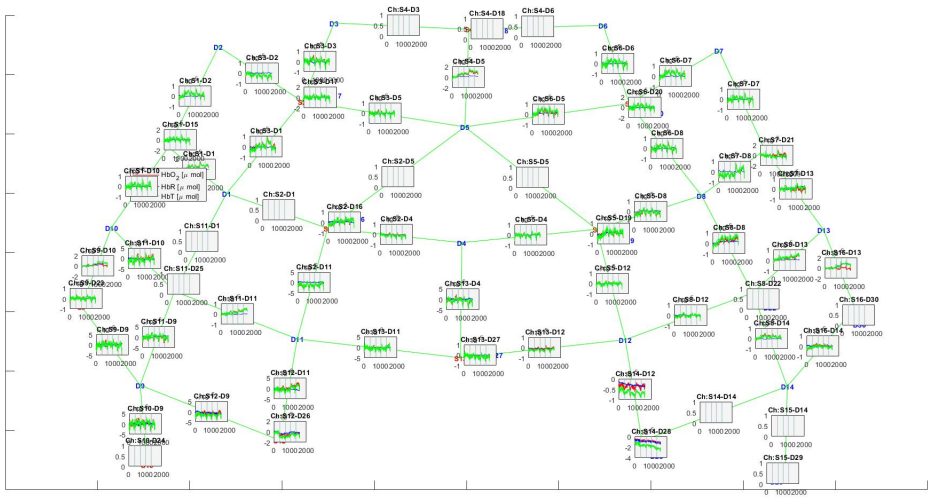

Figure 3.7: The converted optical density, where the red line represents the oxygenated haemoglobin concentration (HbO), the blue line represents the deoxyhemoglobin concentration (HbR), and the green line represents the total hemoglobin concentration (HbT). Blank windows represent bad channels that have been removed during the processing phase.

series needs to be removed before analyses can be performed. The reason is that the expected estimated beta is unbiased, which means that the autocorrelation given to the signal by physiological processes has to be reduced. Therefore, a common method is to calculate the regressor coefficients at first, the AR(p) model was fitted to the residual series and then

$$Y^* = Y_t - \rho Y_{t-1}, X^* = X_t - \rho X_{t-1} \tag{3.1}$$

reduce the effect of the signal at the previous time point on the signal at the present time point Plichta et al. (2007). Finally β was recalculated and a t-test was done for all slopes on each stimulus line for each channel to determine the influence of the independent variable on the dependent variable. When doing single subject significance tests, compare β to 0 and do hypothesis testing. In the hypothesis, H0: $\beta = 0$, i.e., the stimulus has no effect on brain activity, and H1: $\beta \neq 0$, i.e., the stimulus has an effect on brain activity. The above approach is applicable to the GLM model, while the ER model is a bit more complex.

The ER model has seven columns in the design matrix for each channel, with each stimulus line associated to three betas, which means a few more steps in between. In the ER model, the linear model composition for each signal point is

$$y_i = \beta_0 + \beta_1 x_1 + \beta_2 x_1^{'} + \beta_3 x_1^{''} + \beta_4 x_2 + \beta_5 x_2^{'} + \beta_6 x_2^{''}. \tag{3.2}$$

So for each time point, the corresponding seven slopes are obtained. As described in the GLM model section, after the initial β calculation, it is necessary to remove the autocorrelation and perform a secondary β calculation. Then in order to focus only on the effect of the stimulus line of interest, set up a contrast matrix. For example, when investigating the effect of stimulus 1 on brain activity signals,

$$C = [1, 1, 1, 0, 0, 0, 0], \tag{3.3}$$

which means focusing only on the data related to stimulus 1. Each signal time point can be represented by a function containing HRF, the first derivative of HRF and the second derivative of HRF. This can be seen as an expansion term of a Taylor's formula:

$$F(x) = b_3 * f(x_0) + b_2 * d^{'} f(x_0) + b_1 * d^{''} f(x_0) + \varepsilon. \tag{3.4}$$

The contrast matrix has a large range of free choices, referring here to Taylor's formula

$$C = [1, \frac{1}{2!}, \frac{1}{3!}, 0, 0, 0, 0]. \tag{3.5}$$

The three slopes at each time point can be combined into a single contrast to conduct the t-test based on the contrast matrix. The subsequent steps are as described in the GLM modelling section.

For synthetic data, after conducting t-tests on the slopes of the regressions using both the GLM model and the ER model, the difference in p-values for each stimulus line and each channel between the two models were compared. Heat maps were plotted to observe the decoupling abilities of both models. When the p-value was lower than 0.05, the null hypothesis was rejected indicating that the stimulus line had a significant impact on the brain area channels. When the p-value exceeded 0.05, the null hypothesis was accepted the null hypothesis was accepted, suggesting that the brain area channels did not significantly respond to the stimulus.

For real experimental data the same method as described above was utilized to analyze and produce the heat map. There are three stages of 'Pre', 'Post', and 'Retention' for individual subjects, and in addition to comparing the p-values of the single subject t-tests, one should also note the single subject differences in measurements between stages.

Chapter 4

Results

This section presents the output results of the steps detailed in the prior section. The implemented ER model was validated using synthetic data. A comparison between the two models was also illustrated by plotting the heat map using data from the actual device. Ultimately, box plots were designed to showcase the variations in p-value distributions at different stages for the same subject.

4.1 synthetic data

Heat maps were created to depict the p-values of the active weights for each channel and stimulus line across both models. As shown in Figure 4.1, the significance test outcomes between the GLM and ER models for the same signals and stimulus lines differed greatly. In the design of the synthetic data, channel 1 is located in a brain region that responds to both stimulus lines, channel 2 is located in a brain region that responds only to stimulus line 1, channel 3 is located in a brain region that responds only to stimulus line 2, and channel 4 is located in a brain region that does not respond to either stimulus line. In the GLM model, all p-values of eight significance tests exceeded 0.05. In contrast, for the ER model, p-values for all intentionally active channels were below 0.05.

4.2 Data acquired by fNIRS instruments

On the basis of the previous section, the p-value of β across all channels of each subject was calculated for all three sessions under different stimuli. The mean p-

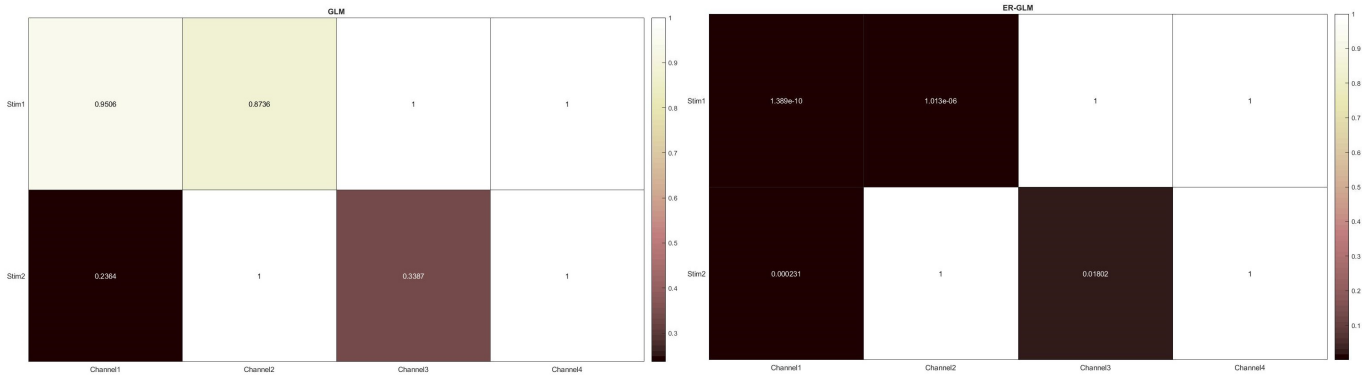

((a)) P-value heat map of GLM model ((b)) P-value heat map of ER model

Figure 4.1: The heatmap includes p-values for doing significance tests for each stimulus line for each channel of the synthesised signal.

values for the three sessions are shown in Table 4.1. As shown in the table, in the comparison between the mean p-values of the three sessions for the two models, the channel of the ER model clearly has a lower p-value.

However, not all subjects performed better in the ER model such as stimulus 1 for subject 19 and stimulus 2 for subject 23. The box plots of p-values for all subjects of the GLM and ER models were shown on Figure 4.2 based on the previous chapter. Subsequent figures show two specific examples: stimulus 1 for subject 11 and stimulus 2 for subject 23. In the two box plots for subject 11, the ER model has a tighter box, whereas for subject 23, the GLM model's box plot is broader.

Further observations were made to make comparisons within the model as Figure 4.2. Table 4.2 demonstrate the sessions variance of each subject between both models to disctibe the degree of deviation of β activation in the three phases. Corresponding to table 4.1, the three medians of the ER model were closer in subject 11. In addition, the interquartile ranges (IQRs) for the different stages were also close. Similarly, in subject 23, the IQRs of the different stages in the GLM model were close, but the medians of the three stages were not significantly different in either model.

Further, the p-value contrast heatmaps for each subject, using both the ER model

	ER						GLM					
	Stim 1			Stim 2			Stim 1			Stim 2		
Subject	Pre	Post	Re	Pre	Post	Re	Pre	Post	Re	Pre	Post	Re
1	0.39	0.24	0.33	0.24	0.44	0.27	0.45	0.33	0.40	0.28	0.31	0.34
2	0.40	0.19	0.13	0.20	0.18	0.20	0.41	0.36	0.10	0.42	0.60	0.19
3	0.28	0.36	0.27	0.27	0.33	0.26	0.30	0.34	0.31	0.36	0.28	0.23
4	0.26	0.41	0.15	0.34	0.45	0.15	0.47	0.62	0.14	0.44	0.55	0.24
5	0.31	0.38	0.30	0.23	0.34	0.25	0.27	0.39	0.30	0.28	0.30	0.23
6	0.32	0.29	0.30	0.33	0.31	0.24	0.29	0.35	0.30	0.28	0.33	0.30
7	0.31	0.33	0.23	0.24	0.32	0.20	0.28	0.37	0.30	0.37	0.38	0.29
8	0.39	0.21	0.31	0.40	0.20	0.30	0.33	0.43	0.40	0.39	0.28	0.18
9	0.22	0.28	0.30	0.21	0.28	0.27	0.26	0.25	0.39	0.27	0.30	0.29
10	0.31	0.26	0.28	0.19	0.20	0.35	0.33	0.29	0.42	0.22	0.28	0.39
11	0.22	0.23	0.24	0.29	0.24	0.14	0.28	0.34	0.44	0.46	0.27	0.48
12	0.18	0.24	0.25	0.23	0.33	0.21	0.16	0.31	0.41	0.25	0.37	0.37
13	0.28	0.49	0.34	0.40	0.22	0.29	0.21	0.46	0.32	0.44	0.52	0.55
14	0.25	0.24	0.19	0.17	0.35	0.30	0.22	0.40	0.19	0.17	0.31	0.32
15	0.18	0.18	0.19	0.30	0.26	0.26	0.19	0.15	0.41	0.60	0.30	0.58
16	0.24	0.21	0.26	0.21	0.28	0.17	0.25	0.20	0.35	0.27	0.35	0.33
17	0.23	0.24	0.27	0.27	0.25	0.17	0.27	0.17	0.31	0.19	0.23	0.31
18	0.32	0.35	0.20	0.34	0.34	0.20	0.31	0.29	0.21	0.29	0.27	0.20
19	0.17	0.26	0.23	0.27	0.21	0.24	0.14	0.22	0.19	0.15	0.26	0.38
20	0.17	0.33	0.18	0.26	0.28	0.14	0.16	0.32	0.29	0.18	0.36	0.23
21	0.27	0.34	0.23	0.25	0.31	0.20	0.32	0.34	0.22	0.19	0.19	0.23
22	0.30	0.25	0.21	0.19	0.28	0.19	0.36	0.31	0.29	0.25	0.13	0.25
23	0.18	0.30	0.31	0.19	0.25	0.24	0.23	0.28	0.41	0.12	0.27	0.13
24	0.23	0.19	0.20	0.18	0.21	0.29	0.26	0.25	0.22	0.16	0.30	0.31
25	0.23	0.22	NaN	0.19	0.18	NaN	0.25	0.27	NaN	0.18	0.24	NaN
26	0.30	0.26	0.30	0.32	0.24	0.30	0.38	0.34	0.42	0.28	0.40	0.36
27	0.26	0.40	0.33	0.20	0.19	0.29	0.31	0.30	0.30	0.20	0.16	0.27
28	0.24	0.28	0.33	0.31	0.30	0.29	0.27	0.25	0.33	0.24	0.34	0.29
Mean	0.25	0.28	0.25	0.26	0.28	0.24	0.28	0.32	0.31	0.28	0.32	0.31

Table 4.1: Mean of P-value for each subjects between two models.

and GLM models were generated based on the steps outlined in the previous chapter. For a more detail comparison, Figure 4.3 uses the same two subjects as the box plots. For subject 11, the ER model demonstrated a more significant stimulus response,

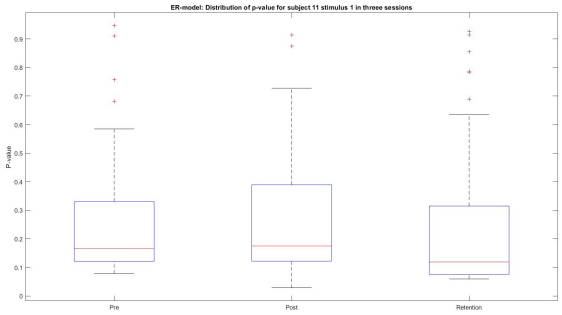

((a)) Box plot of subject 11 stimulus 1 ER model

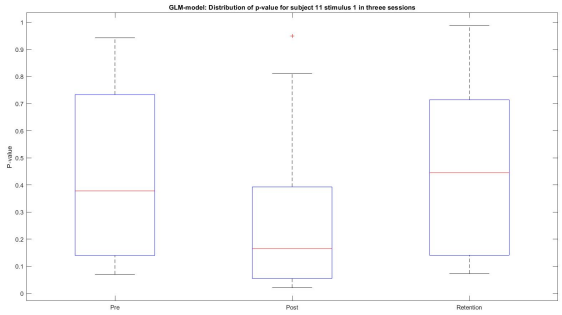

((b)) Box plot of subject 11 stimulus 1 GLM model

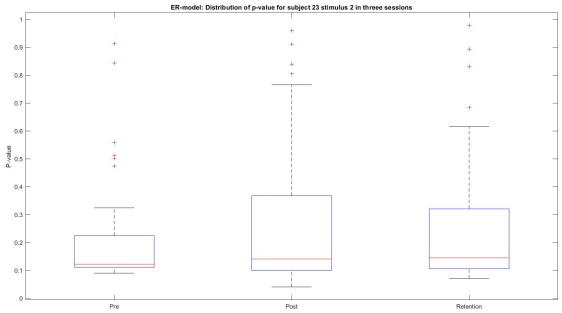

((c)) Box plot of subject 23 stimulus 2 ER model

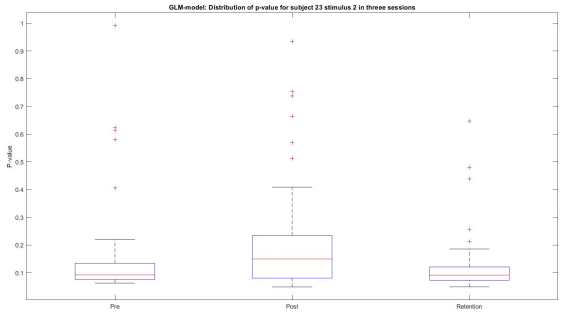

((d)) Box plot of subject 23 stimulus 2 GLM model

Figure 4.2: Comparison of box plots of subject 11 and subject 23 under the two models

	ER model	GLM model
Subject 11	9.0617e-04	0.0214
Subject 23	1.5092e-04	9.1345e-04

Table 4.2: Sessions variances of ER model and GLM model.The table calculates the variance of the median of the three phases of each subject's box plot.

while for subject 23, the channel of the GLM model demonstrated a more significant stimulus effect. The horizontal axis of the graph represents channels, while the vertical axis represents different stages for the same subject. The black sections highlight the channels that were eliminated during preprocessing and thus lack data .

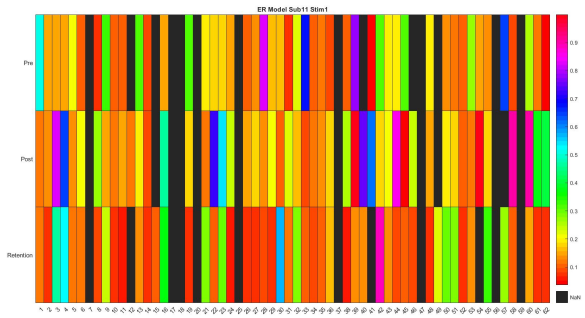

((a)) Heat map of subject 11 stimulus 1 ER model

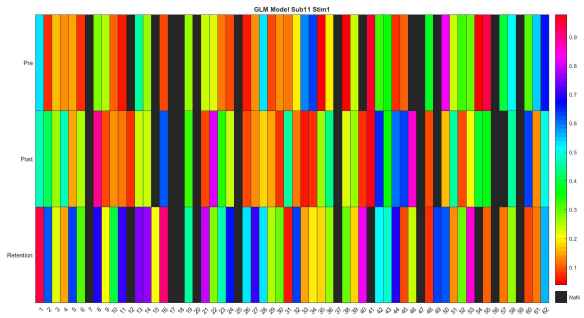

((b)) Heat map of subject 11 stimulus 1 GLM model

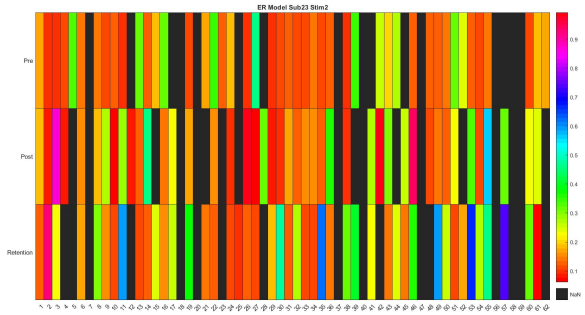

((c)) Heat map of subject 23 stimulus 2 ER model

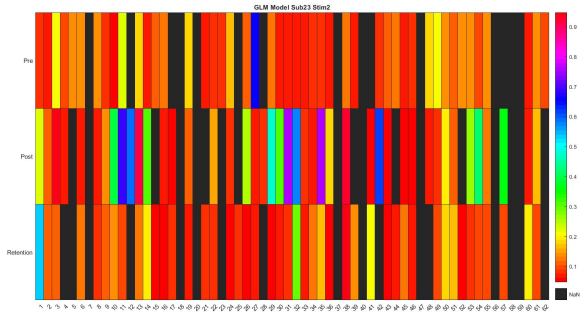

((d)) Heat map of subject 23 stimulus 2 GLM model

Figure 4.3: Comparison of heat maps of subject 11 and subject 23 under the two models. Figures (a) and (b) show the response of subject 11 between the two models under the stimulus 1. There is a very significant difference in the retention phase. Figures (c) and (d) demonstrate the response of subject 23 between the two models under the stimulus 2. A more distinct response is presented within the GLM model.

In the inter-model comparison, it was observed that the overall trend of the two graphs for subject 11 was similar. In the 'Pre' session, the two models have similar p-value distributions, but in the 'Post' and 'Retention' sessions, the regression coefficients of the ER model are more significant and suggesting high channel activity. In contrast, while both models for subject 23 displayed analogous patterns, the GLM model identified several significant channels across all three phases. Conversely, the ER model presented a generally higher p-value.

Subsequent comparisons evaluated the different stages within each model. The model

that performed less optimally for each subject exhibited different channel activity trends across the three sessions. In the GLM model, most of the channels in subject 11 had a clear tendency to be less active in the 'Retention' session than in the other two sessions. Similarly, in the ER model for subject 23, in contrast to the other two sessions, most of the channels had a cooler colour bar in the 'Retention' session, implying that these channels had higher p-values and lower activity.

4.3 Use guide

This section will briefly introduce the use of the code for data processing and model generation. All code and generated images can be found in the git address in the Appendix. All code uploaded in git is original. Matlab 2017b and the open source package Homer3 were used in this project.

1. exe.m: Input the addresses of the raw data (snirf files) for each of the sessions. Select the subjects and call the process.m method to generate the box plot and heat map of the ER model. And output the mean values of all channels for all three sessions for selected subject.

2. process.m: Process the raw data and fit it to the ER model for regression analysis.

3. exeglm.m: Input the addresses of the raw data (snirf files) for each of the sessions. Select the subjects and call the processglm.m method to generate the box plot and heat map of the GLM model. And output the mean values of all channels for all three sessions for selected subject.

4. processglm.m: Process the raw data and fit it to the GLM model for regression analysis.

5. synthetic.m: Generate synthetic data and plot heat maps for both the GLM and ER models, respectively.

4.4 summary

In this section, the ER model implemented into the code is validated and the results of the t-test are consistent with the expected experimental design. In order to assess the participants' responses, a t-test was done on the beta of all channels for each subject to check for changes in activity under different stimulus conditions. The mean of each subject's p-value was then calculated. Then, two typical examples were selected for case studies, which showed box plots and heat maps.

Chapter 5

Discussion

This chapter provides a discussion of the results of the previous chapters. The results from the two models for synthetic and collected data are presented separately. Finally, a brief description of the limitations of this study is given.

5.1 Statistical analyses

5.1.1 synthetic data analysis

Based on the experimental design, both stimulus lines in channel 1, stimulus 1 in channel 2, and stimulus 2 in channel 3 should have a significant activity effect on the brain area. This implies that the p value less than 0.05, leading to a rejection of the null hypothesis and indicating that the regressor coefficients within the channels are significant. However, for the same signals and stimulus sequences, the p-value heat maps of the GLM model and the ER model show great differences. For the GLM model, the p-value of all eight significance tests exceeded 0.05, which means that all eight t-tests accepted the null hypothesis. Whereas the channels in the ER model demonstrate a high level of activity, four of the hypothesis tests have p-values less than 0.05, which is just as expected from the experiment. This is because ER models which incorporate derivatives can adjust for changes in HRF over time (Friston et al., 1998). The first order derivative and the second order derivative represent the rate and curvature of the HRF change, respectively, and both functions can quickly complete a cycle from baseline to rise to fall to return to baseline. When stimuli alternate rapidly, blood oxygen concentration changes rapidly. The highly sensitive changes in the derivative term can quickly capture and keep up with the changes in blood oxygen concentration. Therefore, compared to the classical GLM model,

the ER model provides a superior decoupling of the effects between different stimuli. This is matched with the results of the two model presentations, which sustains that the theory was successfully presented in the code.

5.1.2 fNIRS instrument collected data analysis

Table 4.1 lists the mean p-value of all channels for each subject under different conditions and the mean p-value of all subjects. Overall, the ER model has smaller p-values and isolates the effects of stimuli on brain activity more effectively. In comparisons between models for individual subjects, it is worth noting that although the ER model performed better as a whole, not all subjects were better adapted to the ER model, e.g., stimulus 1 for subject 19 and stimulus 2 for subject 23.

In order to make a horizontal comparison, the previous chapter chose one appropriate subject for each of the ER and GLM models and plotted box plots Figure 4.2 and heat maps Figure 4.3. In the example of the two typical subjects highlighted previously, the two results show a huge difference.

For the ER model of subject 11, it is observed that the box of the p-value box plot is tighter and nearer to 0, and most of the channels in the p-value heat map show an active response. Especially in the retention session, the ER model showed higher sensitivity. This indicates that the missing derivative part of the GLM model fails to capture the rapid changes in blood oxygen concentration. In addition, the ER model showed higher reproducibility compared to the GLM model. Referring to the subjects' mean values for each channel in Table 4.1, the ER model had a similar response in the retention session as the other two sessions, while the GLM model had a lower p-value in the retention phase. In contrast, the opposite is true for Subject 23, where the GLM model has a superior performance both in the box plots and in the heat map.In contrast, the opposite is true for Subject 23, where the GLM model has a superior performance both in the box plots and in the heat map.

The results for subject 23 presented a different position from the previous findings in the literature review (Uga et al., 2014). For this subject, the addition of the derivative term did not improve the model's ability to distinguish different stimuli. This is due to the variability in physiological characteristics between individuals, with different responses to stimuli and different hemodynamic responses between subjects, and therefore the adaptation of the model is different (Zohdi et al., 2021). This could

explain why the ER model was a better fit in subject 11, while the GLM model was a better fit in subject 23. Consequently, the outcomes of the ER and GLM models will not be consistent across different subjects.

5.2 Limitations

This study comes with some limitations.Although the ability of the ER model to separate multiple repetitive stimuli has been validated, this conclusion is not applicable to all subjects. On the other hand, the numerical contrast between the ER model and the GLM model in Table 4.1 is not as strong as the contrast between the synthetic data in Figure 4.1. This may be due to the lack of more detailed processing of the data resulting in too much residual noise.

Chapter 6

Conclusions

This chapter provides a brief overview of the dissertation and responds to the research questions posted in chapter one. At the end, future research directions is given.

This dissertation validates and discusses the implementation of an existing event-related model in code form into an optical neuroimaging data analysis tool. The response of each channel signal to the stimulus was examined by performing a significance test on each sample of synthetic and instrumental acquisition data. To test the effectivity of the models, the results of the single subject regression analyses were carefully compared between both GLM and ER models.

Based on the data analyses and model comparisons performed in the previous chapters, The two research questions posed in Chapter 1 can be answered:

> 1. When multiple stimuli overlap in rapid succession, and regression analyses are conducted using both the GLM model and the ER model as implemented in the code, which model more accurately differentiate the effects of individual stimuli on brain regions?
>
> In all eight hypothesis tests, the p-value obtained for the code implemented GLM model were all greater than 0.05, which means that the original hypothesis was rejected in its entirety. None of the channels in the GLM model exhibited a significant response to the cross stimuli. On the other hand, there were four hypothesis tests in the ER model with p-values less than 0.05, which fit right in with the experimentally designed stimulus sequence. Therefore, it is confirmed that the ER model more precisely differentiates the effects of indi-

vidual stimuli on brain regions when multiple stimuli overlap as expected from theory.

2. Within the actual collected fNIRS data set, when decoupling the active brain signals under multiple stimuli using both the ER model and the GLM model, is there consistency between the two models across different subjects?

Table 4.1 shows the mean values of all channels for each subject between the two models. In most of the subjects, the ER model showed a more active response, which indicates that the results remained consistent across subjects between the two models. For subject 11, most channels in the box plots and heat maps demonstrated a significant response to the introduced stimuli. However, in subject 23, the GLM model showed more channels with high activity. This indicates that despite the ER model has the superior decoupling ability, the fitness of different subjects between the two models could be different.

The present study provides optical neuroscientists with a simpler tool for data analysis and validates its correctness. However, some limitations remain: (1) subjectivity in the processing procedure ; (2) differences in cerebral hemodynamic response between subjects. Future researchers should take both of these points into account, considering researcher subjectivity and individual differences between subjects, so that more precise methods can be used in the analysis of brain imaging data.

Bibliography

[1] Pinti, P. et al. (2020) 'The present and future use of functional near-infrared spectroscopy (FNIRS) for Cognitive Neuroscience', Annals of the New York Academy of Sciences, 1464(1), pp. 5–29. doi:10.1111/nyas.13948.

[2] Quaresima, V., Bisconti, S. and Ferrari, M. (2012) 'A brief review on the use of functional near-infrared spectroscopy (FNIRS) for language imaging studies in human newborns and adults', Brain and Language, 121(2), pp. 79–89. doi:10.1016/j.bandl.2011.03.009.

[3] Yoo, S.-H., Huang, G. and Hong, K.-S. (2023) 'Physiological noise filtering in functional near-infrared spectroscopy signals using wavelet transform and long-short term memory networks', Bioengineering, 10(6), p. 685. doi:10.3390/bioengineering10060685.

[4] Scarpa, F. et al. (2013) 'A reference-channel based methodology to improve estimation of event-related hemodynamic response from fNIRS measurements', NeuroImage, 72, pp. 106–119. doi:10.1016/j.neuroimage.2013.01.021.

[5] Len-Carrin, J. and Len-Domnguez, U. (2012) 'Functional near-infrared spectroscopy (FNIRS): Principles and neuroscientific applications', Neuroimaging - Methods [Preprint]. doi:10.5772/23146.

[6] Weibley, H. et al. (2021) 'FNIRS monitoring of infant prefrontal cortex during crawling and an executive functioning task', Frontiers in Behavioral Neuroscience, 15. doi:10.3389/fnbeh.2021.675366.

[7] Almajidy, R.K. et al. (2020) 'A newcomer's guide to functional near infrared spectroscopy experiments', IEEE Reviews in Biomedical Engineering, 13, pp. 292–308. doi:10.1109/rbme.2019.2944351.

[8] With, L.A. de (2020) Using Functional Near-Infrared Spectroscopy to Detect a Fear of Heights Response to a Virtual Reality Environment.

[9] Hocke, L. et al. (2018) 'Automated processing of FNIRS data—a visual guide to the pitfalls and consequences', Algorithms, 11(5), p. 67. doi:10.3390/a11050067.

[10] Pinti, P. et al. (2019) 'Current status and issues regarding pre-processing of fNIRS neuroimaging data: An investigation of diverse signal filtering methods within a general linear model framework', Frontiers in Human Neuroscience, 12. doi:10.3389/fnhum.2018.00505.

[11] Dans, P.W., Foglia, S.D. and Nelson, A.J. (2021) 'Data Processing in functional near-infrared spectroscopy (FNIRS) Motor Control Research', Brain Sciences, 11(5), p. 606. doi:10.3390/brainsci11050606.

[12] Brigadoi, S. et al. (2014) 'Motion artifacts in functional near-infrared spectroscopy: A comparison of motion correction techniques applied to real cognitive data', NeuroImage, 85, pp. 181–191. doi:10.1016/j.neuroimage.2013.04.082.

[13] Friston, K.J. et al. (1998) 'Event-related fmri: Characterizing differential responses', NeuroImage, 7(1), pp. 30–40. doi:10.1006/nimg.1997.0306.

[14] Tak, S. and Ye, J.C. (2014) 'Statistical analysis of FNIRS DATA: A comprehensive review', NeuroImage, 85, pp. 72–91. doi:10.1016/j.neuroimage.2013.06.016.

[15] Schroeter, M.L. et al. (2004) 'Towards a standard analysis for functional near-infrared imaging', NeuroImage, 21(1), pp. 283–290. doi:10.1016/j.neuroimage.2003.09.054.

[16] Heilbronner, U. and Münte, T.F. (2013) 'Rapid event-related near-infrared spectroscopy detects age-related qualitative changes in the neural correlates of response inhibition', NeuroImage, 65, pp. 408–415. doi:10.1016/j.neuroimage.2012.09.066.

[17] Mayer, A.R. et al. (2014) 'Investigating the properties of the hemodynamic response function after mild traumatic brain injury', Journal of Neurotrauma, 31(2), pp. 189–197. doi:10.1089/neu.2013.3069.

[18] Zhang, D. et al. (2017) 'Discrimination of emotional prosodies in human neonates: A pilot fnirs study', Neuroscience Letters, 658, pp. 62–66. doi:10.1016/j.neulet.2017.08.047.

[19] Li, E. et al. (2021) 'Positive emotion of self-referential contexts could facilitate adult's novel Word learning: An fnirs study', Brain and Language, 221, p. 104994. doi:10.1016/j.bandl.2021.104994.

[20] Maidan, I. et al. (2015) 'Changes in oxygenated hemoglobin link freezing of gait to frontal activation in patients with parkinson disease: An FNIRS study of transient motor-cognitive failures', Journal of Neurology, 262(4), pp. 899–908. doi:10.1007/s00415-015-7650-6.

[21] Çiftçi, K. et al. (2008) 'Constraining the general linear model for sensible hemodynamic response function waveforms', Medical amp;amp; Biological Engineering amp;amp; Computing, 46(8), pp. 779–787. doi:10.1007/s11517-008-0347-6.

[22] Zohdi, H., Scholkmann, F. and Wolf, U. (2021) 'Individual differences in hemodynamic responses measured on the head due to a long-term stimulation involving colored light exposure and a cognitive task: A spa-fnirs study', Brain Sciences, 11(1), p. 54. doi:10.3390/brainsci11010054.

[23] von Lühmann, A. et al. (2020) 'Using the general linear model to improve performance in fNIRS single trial analysis and classification: A perspective', Frontiers in Human Neuroscience, 14. doi:10.3389/fnhum.2020.00030.

[24] Plichta, M.M. et al. (2007) 'Model-based analysis of rapid event-related functional near-infrared spectroscopy (NIRS) data: A parametric validation study', NeuroImage, 35(2), pp. 625–634. doi:10.1016/j.neuroimage.2006.11.028.

[25] Uga, M. et al. (2014) 'Optimizing the general linear model for functional near-infrared spectroscopy: An adaptive hemodynamic response function approach', Neurophotonics, 1(1), p. 015004. doi:10.1117/1.nph.1.1.015004.

[26] Ozawa, T. et al. (2013) 'Detecting event-related motor activity using functional near-infrared spectroscopy', 2013 6th International IEEE/EMBS Conference on Neural Engineering (NER) [Preprint]. doi:10.1109/ner.2013.6696237.

[27] YE, J. et al. (2009) 'NIRS-SPM: Statistical parametric mapping for near-infrared spectroscopy', NeuroImage, 44(2), pp. 428–447. doi:10.1016/j.neuroimage.2008.08.036.

[28] Smith, C. (2023) New Brite MkIII Wearable and Wireless fNIRS system, Cortech Solutions, Inc. Available at: https://cortechsolutions.com/new-brite-mkiii-wearable-and-wireless-fnirs-system/ (Accessed: 01 September 2023).

[29] Barati, Z. et al. (2012) 'Hemodynamic response to repeated noxious cold pressor tests measured by functional near infrared spectroscopy on forehead', Annals of Biomedical Engineering, 41(2), pp. 223–237. doi:10.1007/s10439-012-0642-0.

[30] Izzetoglu, M. et al. (2007) 'Functional brain imaging using near-infrared technology', IEEE Engineering in Medicine and Biology Magazine, 26(4), pp. 38–46. doi:10.1109/memb.2007.384094.

[31] Cignetti, F. et al. (2016) 'Pros and cons of using the informed basis set to account for hemodynamic response variability with developmental data', Frontiers in Neuroscience, 10. doi:10.3389/fnins.2016.00322.

Appendix A

The git address is: https://git.cs.bham.ac.uk/projects-2022-23/yxw537

The git address contains five methods and two zip archives. Matlab 2017b and the open source toolkit Homer3 are required to run. All code uploaded is my own original work.

The ER heatmaps and GLM heatmaps contain heat maps of both models for all subjects.

The exe.m function and process.m function process and fit the data to the ER model.

The exeglm.m function and processglm.m function process and fit the data to the GLM model.

Synthetic.m generates synthetic data and fits to both models.